Studies in Surface Science and Catalysis 160
P.L. Llewellyn, F. Rodriquez-Reinoso, J. Rouqerol and N. Seaton (Editors)
© 2007 Elsevier B.V. All rights reserved

Confinement effects on freezing of binary mixtures

Benoit Coasne[a,b], Joanna Czwartos[c], Keith E. Gubbins[a], Francisco R. Hung[a] and Malgorzata Sliwinska-Bartkowiak[c]

[a] Center for High High Performance Simulation and Department of Chemical and Biomolecular Engineering, North Carolina State University, Raleigh, NC 27695-7905, USA

[b] Laboratoire de Physicochimie de la Matière Condensée, CNRS (UMR 5617) and University Monpellier 2, Place Eugène Bataillon, 34095 Montpellier Cedex 05, France

[c] Institute of Physics, Adam Mickiewicz University, Umultowska 85, 61-614 Poznan, Poland

We report molecular simulations and experimental measurements of the freezing and melting of mixtures confined in nanopores. Dielectric relaxation spectroscopy was used to determine the experimental phase diagram of mixtures confined in activated carbon fibers. Grand Canonical Monte Carlo simulations combined with the parallel tempering technique were used to model the freezing of several Lennard – Jones mixtures in graphite slit pores. The effect of confinement is discussed for mixtures having a simple solid solution or an azeotropic solid – liquid phase diagram. We also investigate how the competition between the wall – fluid and fluid – fluid interactions affects the freezing temperature of the confined system. The structure of the crystal phase in the simulations is also investigated by means of positional and bond-orientational pair correlation functions and bond-order parameters.

1. INTRODUCTION

Many experiments and molecular simulations of the freezing of fluids confined in nanoporous solids have been reported [1]. This effort is devoted to the understanding of the effect of confinement, surface forces, and reduced dimensionality on the thermodynamics of fluids. These works are also of practical interest for applications involving confined systems (lubrication in nanotechnologies, synthesis of nano-structured materials, phase separation, etc). Beside the abundant literature for pure fluids in nanopores, few studies [2-7] have focused on the freezing of confined mixtures. As in the case of pure substances, the pore width H and the ratio of the wall/fluid to the fluid/fluid interactions (parameter α [8]), play an important role in the phase behavior of the mixture. The ratio of the wall/fluid interaction for the two species is also a key parameter in describing freezing of these systems.

In this paper, we review our experimental and simulation work [5-7] and include new results on the solid – liquid phase behavior of mixtures confined in nanopores. Dielectric relaxation spectroscopy (DRS) was used to study the experimental phase diagram of CCl_4/C_6H_{12} mixtures confined in activated carbon fibers (ACF). Grand Canonical Monte Carlo (GCMC) simulations with the parallel tempering technique were used to model the freezing of Lennard-Jones mixtures in slit pores. Mixtures having a simple solid solution or

an azeotropic solid-liquid phase diagram were considered. We also investigate the effect of the ratio α of the wall-fluid to the fluid-fluid interactions on the freezing temperature of the confined system. The structure of the crystal phase is also discussed using both positional and bond-orientational pair correlation functions and bond-order parameters.

2. EXPERIMENTAL AND SIMULATION METHODS

2.1. Experiment

ACF with a pore width of 1.2 nm was used to study freezing of confined CCl_4/C_6H_{12} mixtures. Pores in this material, which are approximately of a slit geometry, are expected to accommodate two layers of CCl_4 or C_6H_{12} since the reduced pore width is $H^* \sim 2.4$. DRS was performed using a parallel plate capacitor of empty capacitance $C_0 = 69.1$ pF. The capacitance C and the tangent loss tan(δ) (where δ is the angle by which current leads the voltage) of the filled sample were measured at different temperatures using a SI 1260 impedance/gain phase analyzer in the frequency range 10 Hz – 10 MHz. The real and imaginary parts of the dielectric permittivity $\varepsilon^* = \varepsilon' - i\varepsilon''$ are related to C and δ, $\varepsilon' = C/C_0$ and $\varepsilon'' = \tan(\delta)/\varepsilon'$ [9]. Melting can be monitored in DRS by a large increase in ε'. The sample was introduced in the capacitor as a suspension of ACF filled with the mixture in the bulk mixture. As a result, the measurements yield an effective permittivity that has contributions from the bulk and confined mixtures. Full details regarding the experiments can be found in Ref. [7].

2.1. Molecular simulation

The phase diagram of the bulk and confined mixtures AB were determined using the Gibbs-Duhem integration (GDI) technique [10,11] and GCMC simulations [12], respectively. The GDI consists of determining the phase coexistence conditions by integrating the Clapeyron equation at constant pressure. Such a method allows one to find the relation $T(\xi_B)$ that describes the solid/liquid coexistence temperature when the fugacity fraction for species B, ξ_B, varies from 0 to 1. At each coexistence condition, Monte Carlo simulations in the $NPT\xi_B$ ensemble are performed to estimate the enthalpies and mole fractions for the liquid and solid phases. The GDI and $NPT\xi_B$ Monte Carlo algorithms used in this work are similar to those developed by Hitchcock and Hall [7,11].

The GCMC technique consists of simulating a system having a constant volume V (the pore with the confined phase) in equilibrium with a fictitious reservoir of particles imposing its chemical potentials μ_A, μ_B and its temperature T. We combined the GCMC simulations with a parallel tempering technique to improve the sampling of phase space [12,13]. The input parameters, $\mu_A(T)$ and $\mu_B(T)$ at $P = 1$ atm, were determined using the equation of state for Lennard – Jones mixtures of Johnson *et al.* [14]. Starting with well-equilibrated configurations, we performed GCMC simulations with the parallel tempering technique. 16 replicas were used in each run and the temperature difference between two successive replicas is $\Delta T = 3$ K. After equilibration, density profiles, order parameters, and correlation functions were averaged in a second run. Full details regarding the methods can be found in Refs. [5,7].

The fluid/fluid interactions were modeled using Lennard-Jones potentials with parameters that reproduce properties of the bulk liquids. The cross-species A/B parameters were calculated using the Lorentz-Berthelot combining rules [15]. The slit pore was described as an assembly of two structureless parallel walls. Periodic boundary conditions were applied in the directions parallel to the pore walls. The fluid/wall interaction was calculated using the Steele '10-4-3' potential [16]. The fluid/wall parameters, $\varepsilon_{w/X}$, $\sigma_{w/X}$ (X = A or B) were

determined by combining the wall/wall and fluid/fluid parameters using the Lorentz-Berthelot rules with the values $\varepsilon_{ww}/k_B = 28$ K and $\sigma_{ww} = 0.34$ nm for the carbon wall.

Strong layering of the confined system was observed due to the interaction with the attractive pore walls. The structure of the confined mixture was investigated by calculating for each layer i the 2D bond-order parameters $\Phi_{n,i}$ (n = 4 and 6 for a square and triangular structure, respectively). $\Phi_{n,i}$ was determined as the average value of the local order parameter $\Psi_{n,i}(\mathbf{r})$, which measures the bond order at a position $\mathbf{r}$ of a particle in the layer i [17]:

$$\Phi_{n,i} = \frac{\left|\int \Psi_{n,i}(\mathbf{r})\, d\mathbf{r}\right|}{\int d\mathbf{r}} \quad \text{with} \quad \Psi_{n,i}(\mathbf{r}) = \frac{1}{N_b}\sum_{k=1}^{N_b} \exp(in\theta_k) \qquad (1)$$

where θ_k are the bond angles between the particle and each of its N_b nearest neighbors. $\Phi_{n,i}$ is close to 1 for a crystal layer having a triangular (n = 6) or a square (n = 4) structure and close to 0 for a liquid layer. We also monitored the 2D positional and bond-orientational pair correlation functions, $g_i(r)$ and $G_{n,i}(r) = \langle \Psi_{n,i}^*(0)\, \Psi_{n,i}(r) \rangle$. The latter measures the correlations between the local bond-order parameter $\Psi_{n,i}(r)$ at two positions separated by a distance r.

3. RESULTS AND DISCUSSION

3.1. Solid solution mixtures

We first discuss the freezing of solid solution mixture Ar/Kr confined in a graphite slit pore having a width H = 1.44 nm. Density profiles (not shown) show that the slit pore accomodates two contact and one inner layers. The confined mixture always has a larger Kr mole fraction than the bulk. This result is in agreement with previous works for confined mixtures [18,19], which showed that the mole fraction of the component having the strongest fluid/wall interaction is increased compared to the bulk. The bond-order parameter, Φ_6, for the confined layers of a mixture in equilibrium with a bulk mixture $x_{Kr} = 0.05$ is shown in Fig.1(a) as a function of the temperature T. Φ_6 sharply increases upon freezing at $T \sim 136$ K, which reveals that the confined layers undergo a liquid to crystal phase transition. Φ_6 varies from ~ 0.08 in the liquid region up to ~ 0.80 in the crystal region. This latter value suggests that the crystals layers have a hexagonal structure (triangular symmetry) with, however, some defects. The Kr mole fraction of the confined mixture is shown as a function of the temperature in Fig. 1(b). x_{Kr} sharply increases at T = 136 K from 0.57 in the liquid phase up to 0.67 in the solid phase. This analysis provides a first set of crystal/liquid coexistence conditions: T, x_{Kr}(liquid), and x_{Kr}(crystal).

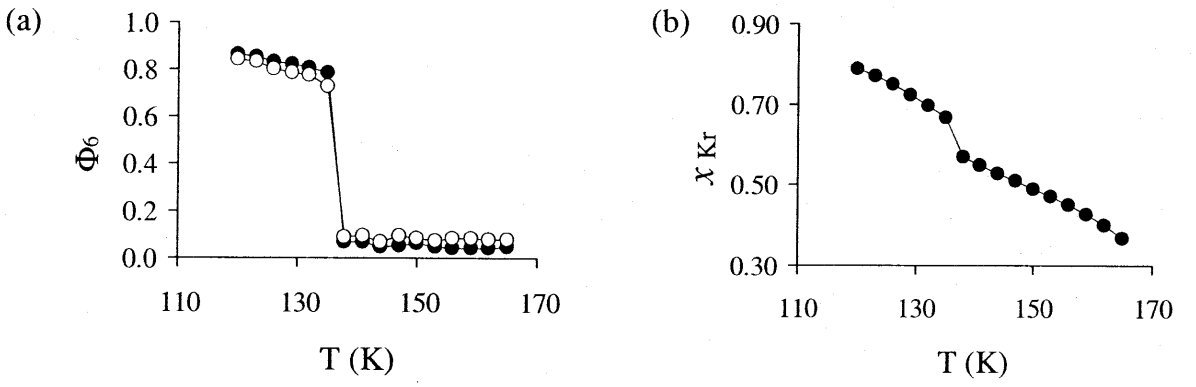

Fig. 1. (a) Φ_6 versus T for Ar/Kr mixtures in a slit pore H = 1.44 nm: (•) contact, (○) inner layers. (b) x_{Kr} versus T for Ar/Kr mixtures in a slit pore H = 1.44 nm.

The freezing temperature for the confined mixture, T_f = 136 K, is much larger than the freezing point of a bulk mixture having the same composition, T_f^{bulk} ~ 111 K [11]. The sharp increase observed in the 2D bond-order parameter Φ_6 and the Kr mole fraction suggest that freezing of the confined layers is a first order transition; however, free energy calculations are required to confirm in a rigorous way the nature of the liquid to crystal transition. Thanks to the use of the parallel tempering technique in which both the liquid and crystal phases are simulated in the same run, we did not perform calculations for the melting process. In our previous work [5,6], it has been shown that simulations of melting and freezing phenomena give similar results, provided that the parallel tempering method is used and a significant fraction of swap moves are accepted [13]. Moreover, Hung *et al.* [20] showed for pure fluids that this technique gives the same results as free energy calculations.

In-plane 2D positional g(r) and orientational $G_6(r)$ pair correlation functions are shown in Figs. 2 and 3 for the contact and inner layers of Ar/Kr confined mixtures in equilibrium with the bulk mixture x_{Kr} ~ 0.05. At T = 129 K, the confined layers appear as 2D hexagonal crystals with long-range positional order as can be seen from the features of the g(r) function for this temperature; the amplitude between the first and second peaks is close to 0, the second peak is split into two secondary peaks, and the third peak has a shoulder on its right side. Moreover, the $G_6(r)$ function at this temperature has a constant average value as expected for a hexagonal crystal layer with long-range orientational order. At T = 144 K, the confined layers exhibit a liquid-like behavior as revealed by the g(R) functions, which are characteristic of a phase having short-range positional order. This result is confirmed by the exponential decay observed in the $G_6(R)$ function; such a decay is typical of 2D liquid phases, which have short-range orientational order. Analysis of the in-plane 2D pair correlation functions corroborate the results shown in Fig. 1(a) for the order parameter Φ_6; the transition temperature between the crystal and liquid phases was found to be T_f ~ 136 K. For all compositions studied in this work, it seems that freezing of the confined layers involves a direct phase transition between a 2D-crystal and a 2D-liquid. This result departs from previous works for confined fluids in which the existence of a hexatic phase between the crystal and liquid phases was reported [21]. Such an intermediate phase is expected according to the KTHNY theory for 2D melting [17]. The stability of the hexatic phase depends on the size of the system, so that the existence of such an intermediate phase cannot be ruled out or confirmed in the present work unless a scaling size analysis is performed [21].

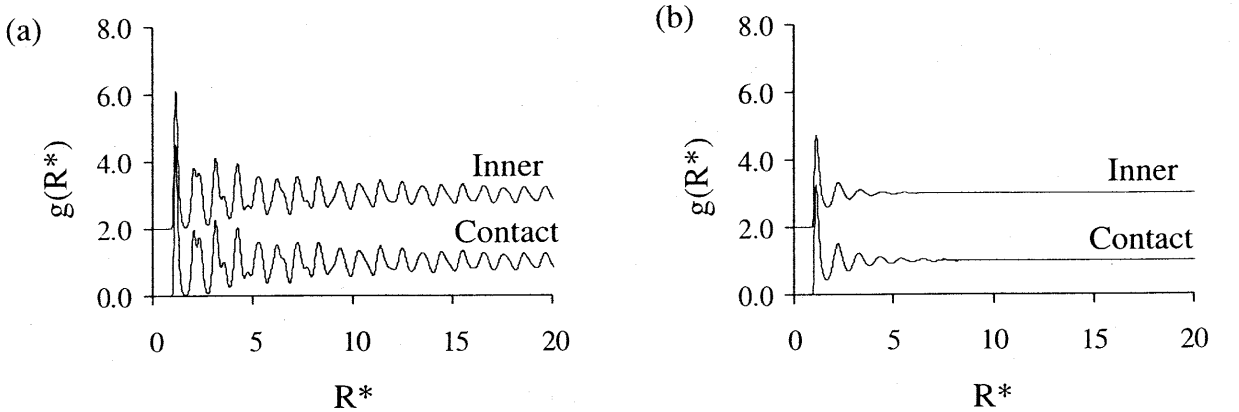

Fig. 2. In-plane 2D pair correlation functions g(R) for the contact and inner layers of Ar/Kr mixtures in a slit pore H = 1.44 nm at (a) T = 129 K and (b) T = 144 K. For the sake of clarity the g(R) function for the inner layer has been shifted by +2. R* is the reduced distance with respect to σ_{Ar}.

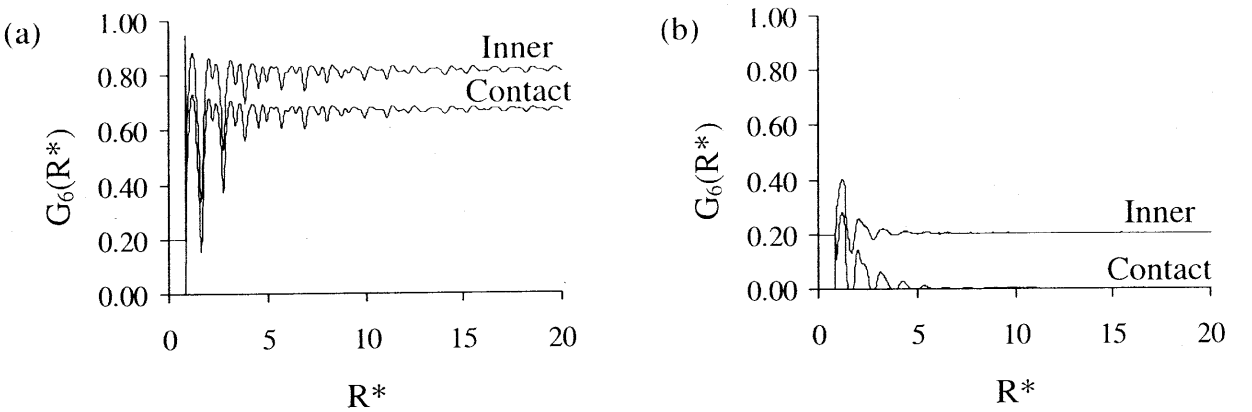

Fig. 3. In-plane 2D pair correlation functions $G_6(R)$ for the contact and inner layers of Ar/Kr mixtures in a slit pore H = 1.44 nm at (a) T = 129 K and (b) T = 144 K. For the sake of clarity the $G_6(R)$ function for the inner layer has been shifted by +0.2. R* is the reduced distance with respect to σ_{Ar}.

The phase diagram (T, x_{Kr}) for Ar/Kr mixtures confined in the 1.44 nm slit pore is shown in Fig. 4(a). The solid/liquid coexistence conditions were determined for different compositions following the analysis described above. Results are compared with the phase diagram obtained for bulk Lennard-Jones Ar/Kr mixtures [11]. The phase diagram for the confined mixture has the same shape as the bulk, but the solid/liquid coexistence lines are shifted to larger temperatures. In agreement with previous works on confined fluids [1,8], this increase in the freezing temperature can be explained by the fact that the ratio of the wall/fluid to the fluid/fluid interactions is larger than 1 for Ar and Kr (α_{Ar} = 1.93, α_{Kr} = 1.78 [5]). We also report in Fig. 4(a) the phase diagram for Ar/Kr mixtures in the 1.44 nm slit pore after an arbitrary reduction of the Ar/wall interaction so that α_{Ar} is lower than 1 (α_{Ar} = 0.80) [6]. In this case, we found that the freezing temperature of the confined system is larger than the bulk for mixtures rich in Kr. In contrast, the freezing temperature for the confined mixture is lower than the bulk for mixtures rich in Ar. Configurations of the contact layer of the confined mixture are shown in Fig. 4(b-c). In each case, the same structure was observed for the inner layer. For all mixtures, the crystal layers have a triangular symmetry, which corresponds to a centered hexagonal structure; this structure is usually observed for strongly attractive pores ($\alpha > 1$) as it corresponds to a dense close-packing of the atoms at the pore wall. In contrast, a square crystal is found for pure Ar in the case of the mixture with α_{Ar} = 0.80; such a symmetry is observed for pore sizes where a change in the number of layers occurs [1].

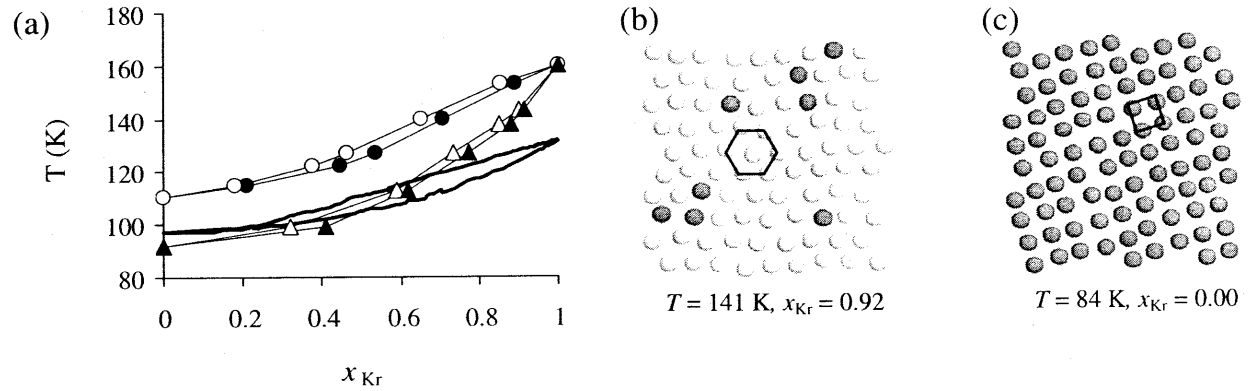

Fig. 4. (a) (○●): (T, x_{Kr}) phase diagram of Ar/Kr mixtures in a pore H = 1.44 nm. Open and closed symbols are the liquid and crystal coexistence lines, respectively. (Δ▲) same as circles but after reduction of the interaction parameter $\varepsilon_{Ar/W}$ from 62.9 K down to 26.1 K (α_{Ar} = 0.80). The thick lines are the phase diagram for the bulk (from [11]). (b),(c) Triangular and square crystals of Ar/Kr mixture in the H = 1.44 nm pore (with α_{Ar} = 0.80). Gray and white spheres are Ar and Kr atoms, respectively.

3.2. Azeotropic mixtures

We now present experiments and molecular simulations for azeotropic mixtures confined in slit pores. Measurements of the dielectric constant $\varepsilon' = C/C_0$ allow the investigation of melting phenomena, as the polarizability of the liquid and solid phases are significantly different [9]. The capacitance curve, C, as a function of the temperature, T, is shown in Fig. 5(a) for a CCl_4/C_6H_{12} mixture with $x_{C6H12} = 0.4$ confined at $P = 1$ atm in ACF with a pore width $H = 1.2$ nm. Melting for both the bulk and the confined mixtures is observed as the sample consists of a suspension of filled ACF in the bulk mixture. A first large increase in the capacitance is observed at $T = -25.0\ ^0C$; this corresponds to the melting temperature of the bulk mixture for $x_{C6H12} = 0.4$. Such an increase at $T = -25.0\ ^0C$ indicates that the bulk crystal mixture starts melting i.e. the system reaches the crystal coexistence line. At $T = -23.3\ ^0C$, the transformation of the bulk crystal into the liquid mixture is complete, i.e. the system reaches the liquid coexistence line, and the capacitance of the system decreases as expected for a liquid phase [9]. This analysis provides both the liquid and crystal coexistence temperatures for bulk CCl_4/C_6H_{12} mixture having a molar composition $x_{C6H12} = 0.4$. At a much higher temperature, $T = 12\ ^0C$, a second increase in the capacitance of the system is observed. The sudden change at this temperature, which does not correspond to any known transition temperature for a bulk CCl_4/C_6H_{12} mixture with $x_{C6H12} = 0.4$, is believed to represent the melting of the material confined within the ACF. As in the case of the bulk mixture, the crystal and liquid coexistence temperatures for this molar composition were estimated from the temperatures where the capacitance starts increasing and where the capacitance reaches a maximum, respectively.

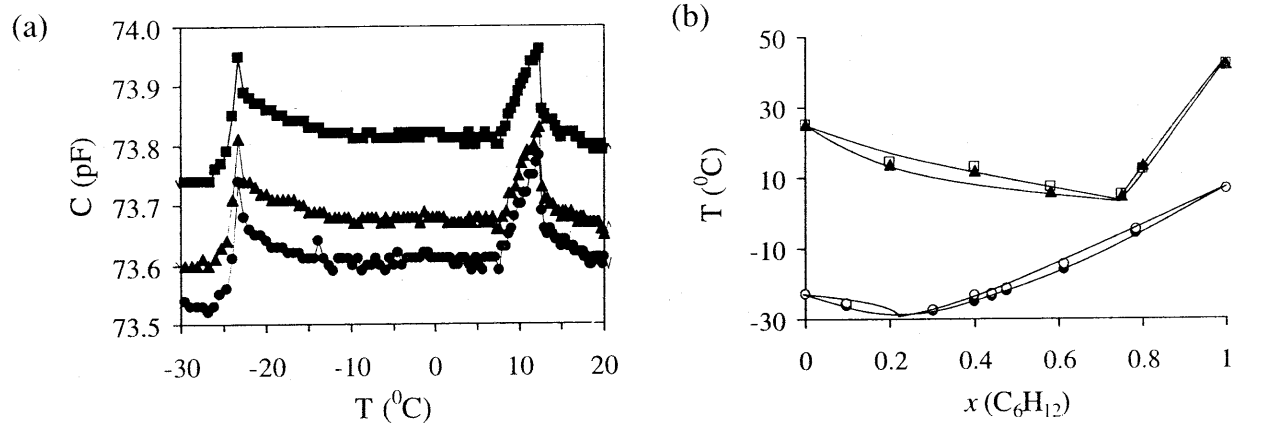

Fig. 5. (a) C versus T curve at $P = 1$ atm for a CCl_4/C_6H_{12} mixture with $x_{C6H12} = 0.4$ confined in ACF ($H = 1.2$ nm): (●) $\omega = 100$ kHz, (▲) $\omega = 600$ kHz, and (■) $\omega = 1$ MHz. The signal is for both the bulk and confined mixtures as the sample is a suspension of filled ACF in the bulk mixture. (b) (T, x_{C6H12}) phase diagram at $P = 1$ atm for CCl_4/C_6H_{12} mixture: (○●) bulk, (□▲) in ACF with a pore width $H = 1.2$ nm. Open and closed symbols are the liquid and crystal coexistence lines, respectively.

The experimental process described above was repeated for different mole fractions in order to obtain the solid/liquid phase diagram for confined CCl_4/C_6H_{12} mixtures (see Fig. 5(b)). The phase diagrams for the confined mixture is of the same type as that for the bulk, i.e. azeotropic, but the solid/liquid coexistence lines are located at higher temperature. The shift in the coexistence conditions is consistent with previous works, which showed that the freezing temperature for systems confined in strongly attractive pores is increased compared to the bulk [1,8]. The relative increase in the freezing temperature is 1.19 for pure CCl_4 and 1.12 for pure C_6H_{12}. The larger shift for CCl_4 can be explained by the larger α value for this

fluid (α_{CCl4} = 1.93, α_{CH4} = 1.76 [7]). We note that the increase in freezing temperature as a function of x_{C6H12} cannot be discussed quantitatively as only the global mole fraction of the sample (bulk and confined) is known. For the same reason, the location of the azeotrope for the confined mixture $x_{0,C6H12} \sim 0.75$, which is larger than the bulk azeotrope $x_{0,C6H12} \sim 0.23$, cannot be discussed.

In order to complement our experimental investigation, we performed GCMC simulations for Ar/CH_4 azeotropic mixtures confined in a slit pore of a width H = 1.02 nm. Such a size was chosen because it corresponds to a similar reduced pore size to that used in the experiments, i.e. $H^* \sim 3$. Density profiles of the confined mixture are shown in Fig. 6(a) for two different temperatures; the confined mixture has a layered structure, composed of two symmetrical layers. In order to obtain the phase diagram for the confined mixture, we performed simulations for different compositions of the bulk mixture. For each run, the liquid/solid coexistence was determined following the analysis described in section 3.1; freezing was monitored through the changes of x_{CH4} and Φ_6 with temperature, and the structure of the confined mixture was studied using both in-plane 2D g(r) and $G_6(r)$ functions. The solid/liquid phase diagram for Ar/CH_4 mixtures in the H = 1.02 nm pore is shown in Fig. 6(b). The confined mixture has the same type of phase diagram as the bulk mixture, but the liquid and crystal coexistence lines are located at higher temperatures. Again, the larger freezing temperature for the confined mixture compared with the bulk can be explained by the fact that both α_{Ar} and α_{CH4} are larger than 1 (α_{Ar} = 2.14, α_{CH4} = 2.16 [7]). The larger increases in the freezing temperatures in the case of the simulations, $T_f^*/\ T_f^{*,bulk} \sim 1.5 - 1.6$, compared to the experiments, $T_f^*/\ T_f^{*,bulk} \sim 1.1 - 1.2$, can be explained by the larger values of the α parameters for the mixtures considered in the simulations [7]. The azeotrope for the confined Ar/CH_4 mixture is located at x_{CH4} = 0.20 and T = 120 K; the crystal for $x_{CH4} < 0.20$ is richer in Ar than the liquid, while the crystal for $x_{CH4} > 0.20$ is richer in CH_4 than the liquid. This situation is similar to that observed for the bulk where freezing involves an increase (decrease) in x_{CH4} for mole fractions above (below) the azeotrope. The simulations for Ar/CH_4 mixtures confined in slit pores are in general agreement with the experiments for CCl_4/C_6H_{12} in ACF; the phase diagram for the confined mixture is of the same type as that for the bulk, but the liquid/crystal coexistence is shifted to higher temperatures.

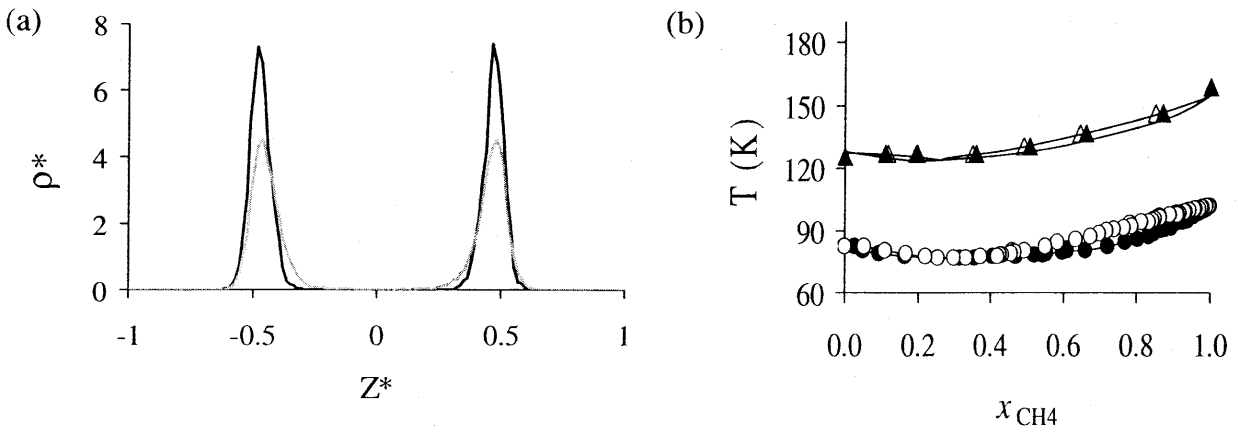

Fig. 6. (a) Density profiles in reduced units $\rho^* = \rho\sigma_{Ar}^3$ of Ar/CH_4 mixture with $x_{CH4} \sim 0.9$ confined in a slit pore H = 1.02 nm: T = 137 K (black line) and T = 163 K (grey line). Z^* is the distance from the pore center in reduced units with respect to σ_{Ar}. (b) (T, x_{CH4}) phase diagram at P = 1 atm for Ar/CH_4 mixtures: (○●) bulk, (Δ▲) in a slit pore H = 1.02 nm. Open and closed symbols denote the liquid and solid coexistence lines, respectively. The lines are provided as a guide to the eye.

4. CONCLUSIONS

Experiments and simulations of the freezing of mixtures confined in nanopores are reported. Mixtures having either a solid solution or an azeotropic phase diagram were considered. In both cases, the phase diagram of the confined mixture is of the same type as that for the bulk. Depending on the ratio α of the wall/fluid to the fluid/fluid interactions, the freezing temperature of the confined mixture is increased ($\alpha > 1$) or decreased ($\alpha < 1$) compared to the bulk. Further studies are needed to corroborate our results. Differential scanning calorimetry should confirm the transition temperatures found in this study, while X-ray diffraction would allow us to determine the structure of the confined phases. Although the use of the parallel tempering technique greatly reduces the risk of being trapped in a metastable state, we plan to combine our simulations with free energy calculations to confirm our findings.

This work was supported by grants from the Petroleum Research Fund (ACS), KBN (PO3B 0114) and NATO (PST.CLG.978802). This research used supercomputing time from HPC-NCSU, SDSC (NSF/MRAC CHE050047S) and NERSC (DOE DE-FGO2-98ER14847).

REFERENCES

[1] For recent reviews, see L. D. Gelb, K. E. Gubbins, R. Radhakrishnan and M. Sliwinska-Bartkowiak, Rep. Prog. Phys., 62 (1999) 1573; H. K. Christenson, J. Phys.: Condens. Matter, 13, (2001) 95; C. Alba-Simionesco, B. Coasne, G. Dosseh, G. Dudziak, K. E. Gubbins, R. Radhakrishnan and M. Sliwinska-Bartkowiak, J. Phys.: Condens. Matter, to be published (2005).
[2] R. R. Meyer, J. Sloan, R. E. Dunin-Borkowski, A. I. Kirkland, M. C. Novotny, S. R. Bailey, J. L. Hutchison and M. L. H. Green, Science 289 (2000) 1324.
[3] M. Wilson, J. Chem. Phys., 116 (2002) 3027.
[4] B. Cui, B. Lin and S. Rice, J. Chem. Phys., 119 (2003) 2386.
[5] B. Coasne, J. Czwartos, K. E. Gubbins, F. R. Hung and M. Sliwinska-Bartkowiak, Mol. Phys., 102 (2004) 2149.
[6] B. Coasne, J. Czwartos, K. E. Gubbins, F. R. Hung and M. Sliwinska-Bartkowiak, Adsorption, 11 (2005) 301.
[7] J. Czwartos, B. Coasne, F. R. Hung, K. E. Gubbins and M. Sliwinska-Bartkowiak, Mol. Phys., in press (2005).
[8] R. Radhakrishnan, K. E. Gubbins and M. Sliwinska-Bartkowiak, J. Chem. Phys., 116 (2002) 1147.
[9] M. Sliwinska-Bartkowiak, J. Gras, R. Sikorski, R. Radhakrishnan, L. D. Gelb and K. E. Gubbins, Langmuir, 15 (1999) 6060; A. Chelkowski, Dielectric Physics, Elsevier, New York, 1980.
[10] M. Mehta and D. A. Kofke, Chem. Eng. Sci., 49 (1994) 2633.
[11] M. R. Hitchcock and C. K. Hall, J. Chem. Phys., 110 (1999) 11433.
[12] D. Frenkel and B. Smit, Understanding Molecular Simulation, Academic Press, New York, 2002.
[13] Q. Yan and J. J. de Pablo, J. Chem. Phys., 111 (1999) 9509.
[14] J. K. Johnson, J. A. Zollweg and K. E. Gubbins, Mol. Phys., 78 (1993) 591.
[15] J. S. Rowlinson, Liquids and Liquid Mixtures, Butterworth Scientific, London, 1982.
[16] W. A. Steele, Surf. Sci., 36 (1973) 317.
[17] B. I. Halperin D. R. and Nelson, Phys. Rev. Lett., 41 (1978) 121; D. R. Nelson and B. I. Halperin, Phys. Rev. B, 19 (1979) 2457; K. J. Strandburg, Rev. Mod. Phys., 60 (1988) 161.
[18] R. F. Cracknell, D. Nicholson and N. Quirke, Mol. Phys., 80 (1993) 885.
[19] Z. Tan and K. E. Gubbins, J. Phys. Chem., 96 (1992) 845.
[20] F. R. Hung, B. Coasne, K. E. Gubbins, E. E. Santiso, F. R. Siperstein and M. Sliwinska-Bartkowiak, J. Chem. Phys., 122 (2005) 144706.
[21] R. Radhakrishnan, K. E. Gubbins and M. Sliwinska-Bartkowiak, Phys. Rev. Lett., 89 (2002) 076101. R. Radhakrishnan, K. E. Gubbins and M. Sliwinska-Bartkowiak, Phys. Rev. B (2005) submitted.